Turkish Journal of Electrical Engineering & Computer Sciences

http://journals.tubitak.gov.tr/elektrik/

Research Article

Turk J Elec Eng & Comp Sci
(2022) 30: 295 – 311

doi:10.3906/elk-2106-3

An active contour model using matched filter and Hessian matrix for retinal vessels segmentation

Mahtab SHABANI[1,*], **Hossein POURGHASSEM**[2]
[1]Faculty of Computer Engineering, Najafabad Branch, Islamic Azad University, Najafabad, Iran
[2]Faculty of Electrical Engineering, Najafabad Branch, Islamic Azad University, Najafabad, Iran

Received: 01.06.2021 • **Accepted/Published Online:** 30.10.2021 • **Final Version:** 19.01.2022

Abstract: Medical image analysis, especially of the retina, plays an important role in diagnostic decision support tools. The properties of retinal blood vessels are used for disease diagnoses such as diabetes, glaucoma, and hypertension. There are some challenges in the utilization of retinal blood vessel patterns such as low contrast and intensity inhomogeneities. Thus, an automatic algorithm for vessel extraction is required. Active contour is a strong method for edge extraction. However, it cannot extract thin vessels and ridges very well. In this research, we propose an improved active contour method that uses discrete wavelet transform for energy minimization to solve this problem. The minimization formula terminates segmentation into two regions, foreground and background. We found out that foreground pixels are more important than background. Therefore, we change the minimization formulation in such a way that gives more weight to the foreground. The contour edge has orientation in each region. The wavelet terms in the minimization formula help to detect edge direction in horizontal, vertical, and diagonal orientations. Since bright and dark lesions do not have direction, these terms can decrease false vessel detection. The second part of the innovation is called the optimization process, which works instead of reinitialization. Sometimes, the evolution in the iterated process destroys the stability of the evolution. To prevent the destruction of the stability of evolution, we used an optimization process formula whose task is to keep contour on the edges of the image. The performance of the proposed algorithms is compared and analyzed on five databases. The values achieved are 94.3%, 73.36%, and 97.41% for accuracy, sensitivity, and specificity, respectively, on the DRIVE dataset, and the proposed algorithm is comparable to the state-of-the-art approaches.

Key words: Retinal vasculature, blood vessel extraction, active contour, Chan-Vese, retinal image segmentation

1. Introduction

A retinal image is achieved by capturing a photograph of the back of the eye. The retinal images are composed of three parts, blood vessel, optic disc, and macula. The vessels have widths of one pixel to twenty pixels [1]. Other items that may appear in these images are pathologies such as in the form of bright and dark lesions. Medical image analysis plays an important role in diagnostic decision support tools. However, manual extraction of the vessels is a difficult and time-consuming task and also requires sufficient skill. There are some vascular characteristics that lead to inaccurate vessel extraction. For example, the intensity of the images is inhomogeneities. Moreover, the contrast of the images is low and the intensity of the vessel pixels can be close to the background pixels. Furthermore, some background features may appear in the image, whose intensity is similar to vessel intensity such as pathologies. These issues warrant an accurate automatic algorithm for vessel

*Correspondence: mahtab_shabani@sco.iaun.ac.ir

extraction. The vessel extraction methods can be divided into multiscale approaches, deformable model, match filtering, and CNN-based approach.

Multiscale approach: The multiscale approach segments blood vessels by different precision. Its advantage is robustness and quick processing [2]. This approach can help us to be more accurate in the algorithm. In the work in [3], multiscale was used for denoising. In [4], line detection is used in multiscale analysis for segmentation. Their approach has three stages. The first stage is the basic line detector. Second multiscale line detectors and last is a combination method. In [5], discrete wavelet transform is integrated with Tyler Coye algorithm to extract the blood vessels. The authors in [6] presented a retinal vessel segmentation method by using the random walk algorithms based on the centerlines. In this work, a Hessian-based multiscale filter is used for vascular enhancement.

Matched filter approach: Another approach used for segmentation is matched filtering. Chaudhuri et al. [7] proposed matched filtering to vessel enhancement. They demonstrated a vascular template determined by Gaussian kernel. Then in [8], Coushy probability distribution is used instead of Gaussian. The authors in [9] demonstrated that vessel template gray level intensity cannot be approximated by Gaussian, and Gumbel distribution is more appropriate than Gaussian. There is a lot of false detection in the matched filter. Because this filter considers nonvessel boundaries as vessels. Zhang et al. [10] proposed the MF-FDOG (matched filter - first-order derivative of Gaussian) to reduce false vessel detection.

CNN: A convolutional neural network (CNN) is a deep learning algorithm that has been introduced as a powerful tool method in segmentation. The authors in [11] used a graphics processing unit implementation of deep convolutional neural networks to separate blood vessels from the background. The authors in [12] consider the graphical structure of vessel shape for segmentation, using both local and global vessel structures. The work in [13] proposed a supervised method by using a wide and deep neural network with strong induction ability to model the transformation.

Deformable model: There is another approach in vessel segmentation entitled deformable models that are also called partial differential equation-based methods. They are divided into snakes, active contour, and level set methods. Some of these methods are region-based and some are edge-based. Edge-based models obtain an object's boundaries using edges information to attract the active contours toward the object. The region-based method includes a region descriptor that the active contour move [14]. Region growing and level set are two favorite methods in this category. The authors in [15] presented a new algorithm based on level set and region growing. Vessels were enhanced by the CLAHE and 2D Gabor wavelet. Then thin vessels are extracted by region growing and the main vessel extracted by the level set method. In [16], a new region-based method is proposed to deal with intensity inhomogeneities in images. The local intensity clustering property was used to formulate the energy formula. There is a neighborhood of each point that global criterion of image segmentation obtains with respect to the neighborhood center. This work was implemented on the MR images of the brain. The results are good on the MRI dataset but it cannot extract weak edges. Papers [17, 18] were proposed specifically for the vessel segmentation problem. The authors in [17] designed an algorithm based on ribbon of twins (ROT). The ribbon of twins is an active contour that one ribbon inside and one ribbon outside captured the vessel. The accuracy of ROT model depends on parameter values. The authors in [18] proposed a new infinite active contour model that segments vessels using different types of region information such as intensity information and local phase-based enhancement map. The infinite perimeter regularizer has more ability to detect small branches compared to the traditional models. Therefore, the vessel detection rate significantly increases. Nevertheless, the background detection rate can decrease with different enhancement filters.

Due to inhomogeneity's intensity, the similarity of the thin vessel intensities to the background pixels and in the presence of pathology spots, vessel segmentation has become a difficult issue. So far, many studies have been carried out to improve the accuracy of vessel detection. However, it is not possible to present an appropriate solution without considering existing issues. The level set method (LSM) is an exact tool for edge extraction in an image. This method is often used for another medical image analyses and is rarely used for retinal vessel segmentation. This is due to the characteristics of the retinal vessels. As noted previously, the intensity of thin vessels is close to the background. In other words, the gradient of edges in the retinal image is low and close to the background. Chan et al. [19] proposed an active contour model that is independent of the gradient of the image and that can be used for retinal images. However, the thin vessels of retinal images can be very close to the background and the CV model [19] cannot extract ridges and weak edges.

According to the approaches mentioned above and the problems and limitations of these methods, it is required to develop an approach that can reduce false detection and increase vessel detection percent. In this work, to increase the true classified rate, we modified the process of the traditional CV model, so that for changes in the process of active contour, we examined what parameters and functions have the most effect on the energy evaluation. One problem of the active contour is the destruction of energy minimization. Therefore, to solve the issue, we use a combination of matched filter and eigenvalue of the Hessian matrix filter called optimization process. The remainder of this paper is organized as follows. In Section 2, the proposed algorithm for retinal vessel segmentation is described in detail. In Section 3, we discuss the performance algorithm and experimental results are presented. Finally, in Section 4, conclusions of the paper and future suggestions are discussed.

2. Proposed segmentation algorithm

Our proposed retinal blood vessel extraction algorithm is a region-based segmentation approach. The block diagram of the proposed approach is shown in Figure 1. The first step is preprocessing by channel selection and contrast limited adaptive histogram equalization. Then to improve the contrast of vessels, an enhancement filter is used. In the next step, modified active contour which optimizes energy formula by adding wavelet terms and optimization process are described. The minimization energy formula is the most important part of active contour. We use the discrete wavelet transformation to improve the performance of the algorithm. The optimized energy formula reduces the effect of noise. In addition, we have added an optimization level to modification of the active contour process. For this work, we use two algorithms to make matrices for use in the optimization process formula. For more information, see Section 2.3.3. Afterward, it is necessary to extract the vessel tree. In this paper, we use the Otsu method for thresholding. Finally, postprocessing is used for false predictions reduction. In what follows, the details of the proposed segmentation algorithm are described.

2.1. Preprocessing

The preprocessing level of the proposed algorithm contains two steps. The first phase of preprocessing is channel selection. The green channel image has a higher contrast between the vessels and the background than the red and blue channels of the RGB color retinal image. Therefore, the green channel of the retinal fundus image is used as the input of the algorithm. To improve the quality of the image, we apply the contrast limited adaptive histogram equalization (CLAHE) on the green channel image, in the second phase of preprocessing.

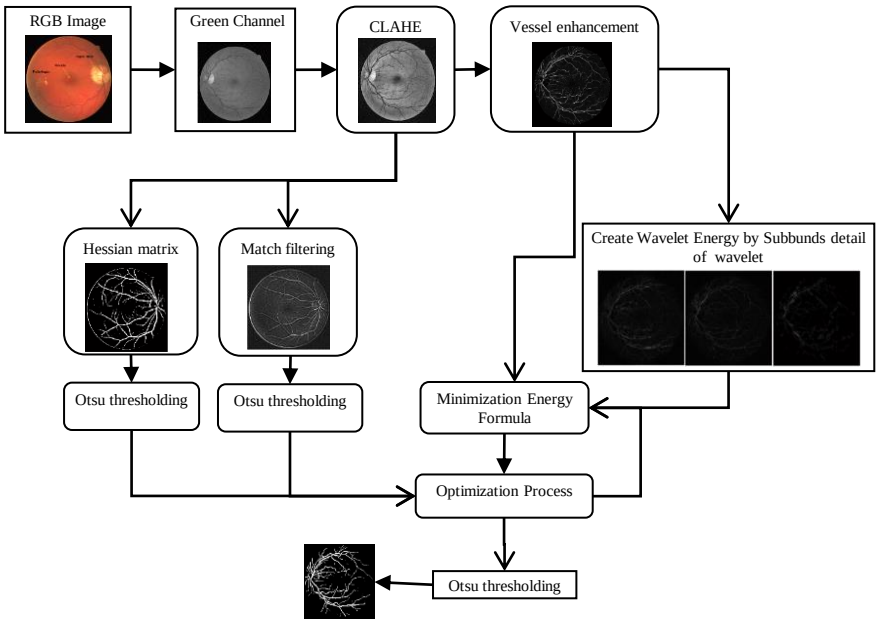

Figure 1. Block diagram of the proposed algorithm.

2.2. Vessel enhancement

After preprocessing, we need an enhancement method of the retinal vessel image. In this work, we use the vessel enhancement method in [20]. The authors in [20] present an algorithm based on iterated morphology operators. This algorithm uses the difference between the supremum and infimum of the opening of the original image with two linear structuring elements of different lengths. They use twelve structuring elements; each element is rotated 15° apart from the previous element. Morphology reconstruction is used to keep small details. A second derivative is used to emphasize thin vessels. There are many reasons for using this filter such as to reduce inhomogeneities illumination and eliminate the false edge around the optic disk.

2.3. Modified active contour

Firstly, we explain some basic knowledge about active contour for readers. Chan-Vese method [19] is a subset of LSM that the Chan-Vese method evolved from Mumford-Shah [21]. CV algorithm is started by initial curve and based on changing formulation to minimization energy. The minimizing energy functional in the CV model is:

$$F(\phi) = \mu(\int_{\Omega} |\bigtriangledown H(\phi)|dx)^p + v\int_{\Omega} H(\phi)dx + \lambda 1\int_{\Omega} |I - C_1|^2 H(\phi)dx + \lambda 2\int_{\Omega} |I - C_2|^2 (1 - H(\phi))dx \qquad (1)$$

where μ, v, $\lambda 1$, and $\lambda 2$ are positive constants. Also $c1$ and $c2$ are two constants; $c1$ is average intensities inside C and $c2$ average is intensities outside C. C is the contour. The first term can be a penalty for contour length. Similarity, second term is a penalty on the sum of the vessels. The third term is the variance of the foreground intensity and measures uniform the light intensity measured by the area. The fourth term does the same for the background. Minimization of the set of the third and fourth term to terminate segmentation

into two regions; each region is uniformly [22]. By minimizing terms, the variational formulation is achieved as follows:

$$\frac{d\phi}{dt} = \delta(\phi)[\mu.div(\frac{\bigtriangledown\phi}{|\bigtriangledown\phi|}) - v - \lambda 1(u_0 - c1)^2 + \lambda 2(u_0 - c2)^2] = 0 \quad (2)$$

where $H(\phi)$ is the Heaviside function used for decision, and $\mu(\phi)$ is the Dirac function that $\delta(z) = \frac{d}{dz}H(z)$. In the following, the modified active contour steps are described.

2.3.1. Initial curve

The active contour method starts with an initial curve. The shape of the initial curve is effective in the growth rate of the algorithm. In our proposed method Canny edge detector is used to make the initial curve shape. Then the closing operator morphology is used. Wide vessels are extracted by the initial contour. This initial contour has some advantages. The number of iterations of the algorithm is significantly reduced. Therefore, the speed of the algorithm is increased and the computational overhead and runtime are decreased. The accuracy of the active contour depends on initial parameters. This initial curve can reduce the dependence of the algorithm with the values of the μ, v. Therefore, these parameters can be set to one.

2.3.2. Wavelet terms

A lot of work has been done to improve the level set formulation. The minimization formula terminates segmentation into two regions, foreground and background. In other researches, the authors paid the same attention to these two regions while the foreground pixels are more important. Therefore, we change the minimization formulation in such a way that gives more weight to the foreground. Discrete wavelet transformation [23] is used in our algorithm. Wavelet transform has many usages in image processing such as compression, reducing the effect of noise, and feature extraction. The wavelet transform decomposes the image into four subbands: approximation and the three detail subbands in the horizontal, vertical, and diagonal directions. The detail subbands keep the intensity variations in the directions of 0, 45, and 90 degrees. The energy functional defined by $F(\phi) = F_{CV}(\phi) + F_{Wavelet}(\phi)$. The wavelet energy ($F_{Wavelet}(\phi)$) is computed by the sum of the following terms:

$$F_{Wavelet_H}(\phi) = \int_{inside(C)|horizontal} u_0(x,y).D_h(x,y)^{1/2}H(\phi(x,y))dxdy$$

$$F_{Wavelet_V}(\phi) = \int_{inside(C)|vertical} u_0(x,y).D_v(x,y)^{1/2}H(\phi(x,y))dxdy$$

$$F_{Wavelet_D}(\phi) = \int_{inside(C)|diagonal} u_0(x,y).D_d(x,y)^{1/2}H(\phi(x,y))dxdy \quad (3)$$

where u_0 is the input image. Equation (3) represent the continuous average values of the root of local wavelet terms. D_h, D_v, and D_d are detail subbands of wavelet that can cover the range of intensity of vessels in the directions of 0, 45, and 90 degrees. $H(\phi(x,y))$ is the Heaviside function that acts on all level curves. It equals $H(\phi(x,y)) = \frac{1}{2}\left(1 + \frac{2}{\pi}\arctan\frac{x}{\epsilon}\right)$. The underlying idea behind the related wavelet terms is as follows: Multiplying the original image (u_0) in the D_h, D_v, and D_d increases the intensity of the wide vascular structure greatly because intensity pixels of wide vessels are higher than thin vessels. Therefore, multiplying two large

numbers gives a larger response. The root of terms reduces the different intensity values between wide vessels and thin vessels because the root operator causes the large numbers to get too small and has less effect on small numbers. The logarithm does the same work. Hence, logarithm (0) = infinite, so we do not use logarithm. The contour edge has direction in each region. The contour edge has orientation in each region. The wavelet terms help to detect edge direction in horizontal, vertical, and diagonal orientations. For as much as, bright and dark lesions do not have direction, these terms can decrease false vessel detection. Therefore, the energy functional from traditional active contour in Equation 1 is rewritten by:

$$F(\phi) = \mu \int_{\Omega} |\bigtriangledown H(\phi(x,y))| dxdy + v \int_{\Omega} H(\phi(x,y))| dxdy + \lambda_1 \int_{inside(C)} |u_0(x,y) - C_1|^2 H(\phi(x,y)) dxdy +$$

$$\lambda_2 \int_{outside(C)} |u_0(x,y) - C_2|^2 (1 - H(\phi(x,y)) dxdy + \lambda_3 \int_{inside(C)|horizontal} u_0(x,y).D_h(x,y)^{1/2} H(\phi(x,y)) dxdy +$$

$$\lambda_4 \int_{inside(C)|vertical} u_0(x,y).D_v(x,y)^{1/2} H(\phi(x,y)) dxdy + \lambda_5 \int_{inside(C)|diagonal} u_0(x,y).D_d(x,y)^{1/2} H(\phi(x,y)) dxdy \quad (4)$$

where μ,v, λ_1, λ_2, λ_3, λ_4, λ_5 are positive constants, and c_1, c_2 are average (u_0) in $\phi_0 >= 0$ and $\phi_0 < 0$, respectively. $\mu \int_{\Omega} |\bigtriangledown H(\phi(x,y))|$ is regarding the total length of edge contour. Similarly, $v \int_{\Omega} H(\phi(x,y))|$ is regarding the total area in the contour. The third and fourth terms are similar to the CV model. Fifth to seventh terms are related to wavelet terms (Equation 3). Finally, the proposed energy fitting minimization can be written:

$$\frac{d\phi}{dt} = \delta_{opt}(\phi)[\mu.div(\frac{\bigtriangledown \phi}{|\bigtriangledown \phi|}) - v - \lambda_1(u_0 - c1)^2 + \lambda_2(u_0 - c2)^2 + \lambda_3(u_0.D_h)^{1/2} + \lambda_4(u_0.D_v)^{1/2} + \lambda_5(u_0.D_d)^{1/2}] = 0 \quad (5)$$

For larger numbers, algorithm gives us a better response although these terms reduce true vascular detection. It is a trade-off for us between higher accuracy and true positive rate. Wavelet terms help to receive upper accuracy. However, it can reduce vessel detection rate.

2.3.3. Optimization process

In the previous section, we used wavelet terms in energy minimization, but wavelet terms can eliminate thin vessels whose directions are different from the wavelet terms orientations. Moreover, sometimes nonvessel structures have high intensity such as pathologies. In such cases, the active contour cannot detect edges good and pathologies parts are considered as vessels. In Figure 2 you see a part of an image that has signs of pathology. In this image, the active contour cannot detect edges good and pathology regions are considered as vessels. In presence of the high intensity in these regions, active contour in the next iterations cannot modify evolution function. Generally, false edge detection happened for one or more of the below reasons: The presence of pathology or intensity inhomogeneities in the image.

Sometimes, the level set function develops irregularities during its evolution and may destroy the stability of the evolution. Therefore, a solution for modification is used that is called 'reinitial', but it is difficult to do. The active contour does not have 'reinitial'. To prevent the destruction of the stability of evolution, we use an

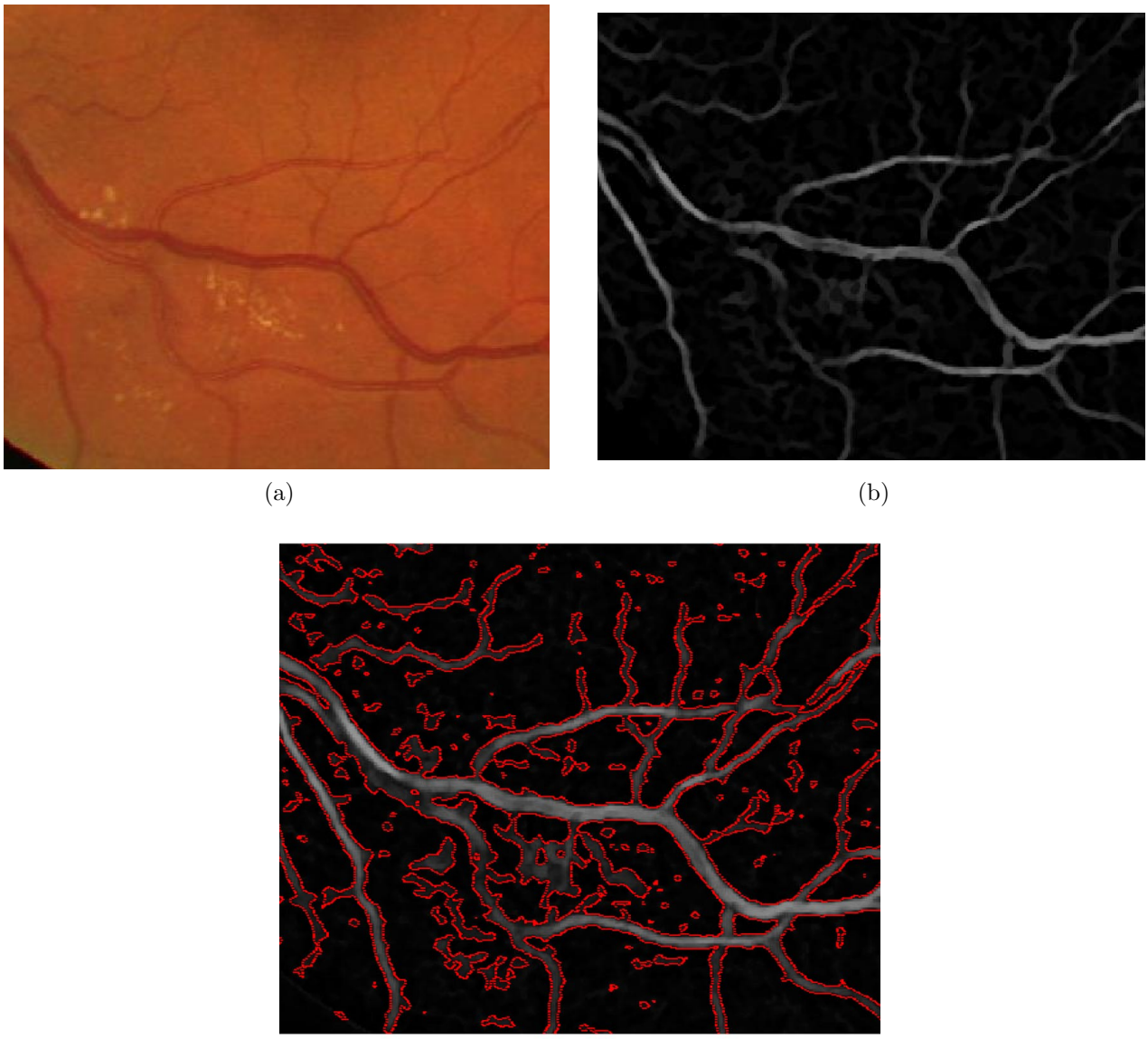

Figure 2. A part of image of DRIVE. (a) the original image, (b) the image after applying enhancement filter, (c) the result of active contour after lot of iterations.

optimization process formula that its task is to keep contour on the edges of the image. The proposed algorithm develops an equation below for modification of evolution function:

$$E_{opt}(x,y) = \alpha_1 E_n(x,y) + \alpha_2 I_{Hess}(x,y) E_n(x,y) + \alpha_3 I_{Mf}(x,y) E_n(x,y) \tag{6}$$

where $\alpha_1 > 0$, $\alpha_2 > 0$, and $\alpha_3 > 0$ are constants that control the priority of each term. E_n is achieved from Equation 7.

$$E_n(x,y) = E_{n-1}(x,y) + \Delta t F(\phi,x,y) \tag{7}$$

where $F(\phi,x,y)$ is energy functional, Δt is time step, and n is number of iterations. E_0 is the initial

curve and its obtained as $E_0(x,y) = \phi_0(x,y)\,\phi(0,x,y)$. I_{Hess} and I_{Mf} in Equation 6 are binary images from Hessian matrix [24] and matched filter [7], respectively. Matched filter considers a model for vessels. It has a 2-D Gaussian kernel and convolves by the main image. The convolution kernel needs to be applied at several rotations. Twelve times the kernel is rotated in 15° increments to fit into vessels of different orientations. The maximum response of the filter is selected for each pixel and then uses a threshold method to provide a binary vessel image. In [24] a vessel enhancement filter by components of Hessian matrix is presented. The Hessian matrix is a square matrix that contains partial second derivatives. These matrixes can be formed by convolutions of image and three second derivatives $Gaussian_x x$, $Gaussian_y y$, and $Gaussian_x y$ as $H(f) = \begin{bmatrix} fxx & fxy \\ fxy & fyy \end{bmatrix}$. Eigenvalues γ_1 and γ_2 are obtained as $\gamma_1 = 1/2(fxx + fyy + temp)$ and $\gamma_2 = 1/2(fxx + fyy - temp)$ that temp is achieved as $temp = \sqrt{(fxx - fyy)^2 + 4f_{xy}^2)}$. The filter is given as:

$$Hess = \begin{cases} 0 & if \gamma_2 > 0 \\ exp(-\frac{R_\beta^2}{2\beta^2})(1 - exp(-\frac{s}{2c^2})) & otherwise \end{cases} \tag{8}$$

where $R_\beta = \frac{\gamma_1}{\gamma_2}$ and $s = \sqrt{\gamma_1^2 + \gamma_2^2}$. Hessian matrix has some properties such as noise elimination, determination of linear structures and spot like. Frangi filter [24] can ignore pathology regions easily. On the other hand, the matched filter has achieved good results for thin vessel detection. Therefore, using the advantages of the filters can improve the active contour result. I_Hess and I_Mf are both binaries. Multiplying I_Hess and $E_n(x,y)$ eliminated the pathologies and noises that the energy function detected as the vessel. However, this term ignores ridges. Matched filtering detects thin vessels very well. To summarize, in Equation 6 we have three results for each pixel (i,j): The first term pointed original pixel in the energy function. The second term replaces zero when the pixel included low intensity or the pixel did not orient. In the third term, the intensity of thin vessels pixels is increased. Set of the probabilities, make an optimal evaluation functional that controls active contour and repair itself in each iteration. Optimal process pulls contour toward the foreground.

2.4. Vessel tree generation

The final step is to extract the vessels tree. There are several methods for classification. In this work, we used simple thresholding with a global threshold level that obtains from Otsu's method [25]. We have two classes of pixels in the vessel segmentation. The pixel (i,j) belongs to the foreground or background. The Otsu algorithm calculates the optimum threshold separating these classes so that their interclass variance is maximal [25]. Optic disc or bright lesions can increase false positives. Moreover, some thin vessels are fragmented. Therefore, the restoration of fragmented-edges and eliminating noise requires postprocessing. For this work, we used morphological operators. Noise pixels are not connected to the vessel tree. Thus, we consider a number as a threshold level and eliminated regions whose number of pixels is less than the threshold. For linking edges, bridge morphologies operator was used. Bridge operator connects pixels, they have two nonzero neighbors.

3. Experimental results and method evaluation

We carry out the algorithm in MATLAB version R2014a on a personal computer running Windows 10 with an Intel(R) Core i5-7200U, the processor 2.5GHz and 8 GB of memory. The proposed algorithm is examined on

the five public available datasets. The DRIVE database [1] contains 40 color retinal images that are divided into two equal parts: a training set and a test set which the training set is used for initialization parameters. We use set A of the manual segmentation at the ground truth. The images of the DRIVE dataset were obtained using a Canon CR5 3CCD camera with a 45-degree field of view, with 8 bits per color plane at 565 by 584 pixels. Notice that the performance of active contour depends on its initial parameter values, and determining parameters is a demanding issue. We set the parameters in such a way that yields good performance. The parameters that should be determined are as follows: Δt, μ, v, λ_1, λ_2, λ_3, λ_4, λ_5, α_1, α_2 and α_3 that λ_3, λ_4, λ_5, α_1, α_2 and α_3 are additional parameters in the proposed active contour. The parameters of μ and v control length and area of contour. μ, v can be set to one due to the special initial curve in the part 2.3.1. Δt is the time step. The lower value of Δt decreases the speed of evaluation and the result of segmentation becomes more reliable. We set it as $\Delta t = 0.001$ by experimenting. λ_1 controls the foreground region and λ_2 acts the same work for background. By increasing the value of λ_1, the true classified rate is decreased and accuracy is increased. The effect of λ_2 is the opposite of λ_1. λ_3, λ_4, λ_5 are constants of wavelet terms. These parameters have the same act of λ_1. We determined these parameters to gain a good value of accuracy and the must thin vessel detection rate. Therefore, it is a trade-off to select the initial values of these parameters. In this work, the best selections are $\lambda_1 = 0.6$, $\lambda_2 = 0.7$, $\lambda_3 = 5$, $\lambda_4 = 5$, $\lambda_5 = 4$. α_1, α_2, and α_3 are related to the optimization process in eq 5. α_1, α_2 and α_3 parameters have a significant effect on segmentation results. Moreover, the effect of all three parameters should be determined together. We examined these values experimentally by changing the values of the parameters on the images of DRIVE. Finally, these set as follows: $\alpha_1 = 0.8$, $\alpha_2 = 0.07$, $\alpha_3 = 0.08$. All parameters of the modified active contour model are given in Table 1.

Table 1. The parameters of the modified active contour model.

$\Delta t = 0.001$	μ =v=1	$\alpha_1 = 0.8$	$\alpha_2 = 0.07$	$\alpha_3 = 0.08$
$\lambda_1 = 0.6$	$\lambda_2 = 0.7$	$\lambda_3 = 5$	$\lambda_4 = 5$	$\lambda_5 = 4$

STARE[2] contains 20 color retinal images, which size of the images is 605 by 700 pixels. We use the hand labeled provided by Hoover at the ground truth. HRF[3] is an image dataset of high-resolution that contains 45 images. This database consists of three groups: 15 healthy patients, 15 patients with diabetic retinopathy, and 15 glaucomatous patients. All images were used for the test. To decrease the computational cost, all images on the HRF dataset were downsampled by a factor of 2. CHASEDB1[4] dataset contains 28 images that Each image is annotated by two independent human observers. We use the hand-labeled provided by observer 1. All images were used for the test. Similarly, ARIA online dataset[5] contained three groups; healthy subjects, diabetic subjects, and age-related macular degeneration subjects. All 59 Diabetic images were used for the test. In the following, the evaluation measures are introduced. Then the proposed algorithm is compared with other work and also compared in the absence of main vessels.

[1]DRIVE (2004). Digital Retinal Images for Vessel Extraction [online]. Website http://www.isi.uu.nl/Research/Databases/DRIVE

[2]STARE (1975). STructured Analysis of the Retina [online]. Website http://cecas.clemson.edu/ ahoover/stare/

[3]HRF (2013). High-Resolution Fundus (HRF) Image Database [online]. Website http://www5.informatik.uni-erlangen.de/research/data/fundus-images/

[4]CHASE DB1 (2011). Retinal image database [online]. Website http://blogs.kingston.ac.uk/retinal/chasedb1

[5]ARIA Online (2006). Retinal Image Archive [online]. Website http://www.eyecharity.com/aria

3.1. Evaluation measures

In the vessel segmentation, we have two classes: vessels and nonvessels. Nine measures are used to evaluate the proposed algorithm: accuracy (ACC), true positive rate, or TPR (vessel pixel counts that true classified), false positive rate (FPR) (nonvessel pixel counts that false classified), sensitivity (SN), specificity (SP), precision (Pr), negative predictive value (NPV), F1, and AUC. Accuracy (ACC) is calculated as the number of all true classified pixels divided by the total number of all pixels. Hence, there are usually background pixels more than vessel pixels, so accuracy measure is not useful to indicate performance, alone. Therefore we use other measures. Sensitivity is calculated as the number of true positive divided by the total number of positives. Specificity (SP) is calculated as the number of true negative pixels divided by the total number of negatives. It is also called the true negative rate (TNR). Precision (Pr) is calculated as the number of true positive pixels divided by the total number of positive predictions. It is also called positive predictive value (PPV). F1 is a harmonic mean between precision and sensitivity. Finally, AUC is a mean between sensitivity and specificity. AUC is a better measure of indicating classification performance. The formulas above are defined as follows:

$$TPR = \frac{TP}{Vesselpixelcount} \quad FPR = \frac{FP}{non-Vesselpixelcount} \quad Acc = \frac{TP+TN}{FOVpixelcount}$$
$$SN = \frac{TP}{TP+FN} \quad SP = \frac{TN}{TN+FP} \quad AUC = \frac{SN+SP}{2}$$
$$PR = \frac{TP}{TP+FP} \quad NPV = \frac{TN}{TN+FN} \quad F1 = \frac{2PR.SN}{PR+SN}$$

The enhancement phase is very important in the performance of segmentation. There are different enhancement filters to highlight vessels. We carried out two enhancement filters on the DRIVE dataset: morphologies filter [20] and Frangi filter [24]. The parameters of the Frangi filter are shown as follows: scales: 1-5, scale ratio:1, $\beta_1 = 0.25$ and $\beta_2 = 5$. However, all of the parameters of [20] were not changed. Their results are shown in Table 2. According to Table 2, it is obvious that morphologies filter [20] gives a better result than the Frangi filter [24]. Therefore, we used [20] to enhancement filter. Table 3 shows the performance measures of the proposed algorithm for the images of DRIVE, STARE, HRF, CHASEDB1, and ARIA datasets, by morphologies filter [20]. The average accuracy, sensitivity, and specificity of DRIVE are achieved 0.943, 0.7336, and 0.9741, respectively. The value of average sensitivity is high and it demonstrates that thin vessels are well detected. Moreover, the value of the average AUC of DRIVE is equal to 0.8539. Pr and NPV of DRIVE are equal to 0.8078 and 0.9612, respectively. The precision metric is the probability that pixels detect as vessels truly be the vessel pixels. Negative predictive value is the probability that pixels detect as nonvessels, truly be the background pixels.

Table 2. Performance of using different enhancement method with the proposed segmentation on the DRIVE.

Enhancement method	Acc	Sn	Sp	AUC
Frangi filter [24]	0.9257	0.6614	0.9645	0.8130
Morphologies filter [20]	0.9430	0.7336	0.9741	0.8539

In addition, the proposed algorithm is analyzed on STARE, HRF, CHASEDB1, and ARIA datasets, in which the average accuracy, sensitivity, and specificity of STARE are achieved 0.9372, 0.7831, and 0.9553, respectively. HRF is a new dataset that is first used in 2013 [26]. The average accuracy, sensitivity, and specificity of all 45 images in the HRF dataset are achieved as 0.9441, 0.7799, and 0.9611, respectively. Table 4 shows the comparison of the work in [26] and our algorithm. The performance of [26] for healthy images is

the same as our approach but the performance of [26] is higher than our algorithm for diabetic retinopathy images. On the other hand, we achieved better performance with glaucomatous images than [26]. The average sensitivity of the ARIA dataset is the lowest of the five databases because we have used diabetic images for the test. In contrast, The CHASEDB1 dataset has the worst false positive rate of the five databases.

Table 3. Performance metrics on the DRIVE, STARE, HRF, CHASE DB1, and ARIA databases.

Performance	TPR	FPR	ACC	SN	SP	Pr	NPV	AUC	F1 score
Mean DRIVE	0.7333	0.0259	0.9430	0.7336	0.9741	0.8078	0.9612	0.8539	0.7649
Mean STARE	0.7829	0.0447	0.9372	0.7831	0.9553	0.6917	0.9743	0.8692	0.7244
Mean HRF	0.7799	0.0375	0.9441	0.7799	0.9611	0.6839	0.9769	0.8705	0.7219
Mean CHASEDB1	0.7876	0.0611	0.9242	0.7928	0.939	0.5905	0.9763	0.8659	0.6721
Mean ARIA online	0.6254	0.0377	0.9317	0.6267	0.9623	0.6344	0.9627	0.7945	0.614

Table 4. Performance of vessel segmentation methods on the HRF database.

	Healthy			Glaucomatous			Diabetic retinopathy		
	Acc	Sn	Sp	Acc	Sn	Sp	Acc	Sn	Sp
Odstrcilik [26]	0.9539	0.7861	0.975	0.9497	0.79	0.9638	0.9445	0.7463	0.9619
Proposed algorithm	0.9516	0.7897	0.9723	0.9515	0.7869	0.9666	0.9292	0.763	0.9446

3.2. Comparison with published methods

In this section, the performance of the proposed algorithm is compared with the papers in the literature. Firstly, it is compared with several active contour methods and then is compared our model with other methods. The active contour models used in this comparison are: Chan-Vese (CV) [19], ROT [17], active contour based on intensity inhomogeneities (ACII) [16] and IPACHI [18]. The results of these comparisons are shown in Tables 5 and 6. We implemented the CV model and ACII model based on the original papers [16, 19], for the DRIVE database. We need to set initial parameters of [16] to using the DRIVE database. Because it was performed for MR images of the brain. To get the best performance, the parameters of the ACII are set as follows: $k \geq (2\sigma)^2 + 1$, $\Delta t = 0.01$, and $\mu = 1$. The parameters of the CV model are set as our algorithm. The results of the ROT and IPACHI are taken from respective original papers [17, 18]. All methods were performed on DRIVE and STARE datasets. The ACII [16] have the worst results because this work was not designed for the retinal images. The results of ROT are close to those our approach. The value of the accuracy of the proposed algorithm is close to that of CV model. The sensitivity and AUC of our approach are better than those of the traditional CV model for DRIVE images. The value of specificity in the Chan-Vese method is higher than that of our method. In contrast, the value of Sn and AUC in the CV model are higher than our method. The IPACHI model is not in Table 5. IPACHI has an enhancement that is different from our enhancement filter. To make a fair comparison, we changed our enhancement phase from [20] to Frangi filter [24]. Therefore, the Frangi filter parameters were set to the same as the values of parameters used in the IPACHI model: Scales are 1-8 and the scale ratio is 2. You can see the results in Table 6. As expected, the performance of the proposed algorithm was reduced by changing the enhancement filter. The accuracy, specificity, and AUC in our approach are better than those of IPACHI on the DRIVE dataset. Just the sensitivity of IPACHI is higher than that

of our approach. In contrast, for the STARE database, IPACHI has better performance of the accuracy and specificity. Overall, our results segmentation is better than that of our competitors.

Table 5. Performance of different active contour methods on the DRIVE and STARE databases.

	DRIVE				STARE			
	Acc	Sn	Sp	AUC	Acc	Sn	Sp	AUC
Chan-Vese [19]	0.9435	0.6905	0.9809	0.8357	0.9309	0.7953	0.9476	0.8714
Intensity inhomogeneities [16]	0.9126	0.6142	0.9566	0.7854	0.9195	0.5874	0.9569	0.7722
ROT [17]	——	0.7282	0.9551	0.8417	——	0.752	0.968	0.860
Proposed algorithm	0.9430	0.7336	0.9741	0.8539	0.9372	0.7831	0.9553	0.8692

Table 6. Performance of two active contour models on the DRIVE and STARE databases.

	Enhancement method	Database	Acc	Sn	Sp	AUC
IPACHI [18]	Frangi filter	DRIVE	0.853	0.686	0.867	0.776
		STARE	0.938	0.634	0.967	0.801
Proposed algorithm	Frangi filter	DRIVE	0.9189	0.6502	0.9583	0.8043
		STARE	0.9287	0.7355	0.9504	0.8429

Previous experiments indicate that our method is comparable to the state-of-the-art active contour models. In this section, we want to make a comparison with other methods. Table 7 shows the performance of our method and the others on the DRIVE, STARE, HRF, and CHASE DB1 datasets. Gao et al. [6] only used the STARE dataset. Frangi and Heneghan were implemented based on the original papers on the DRIVE database. To get the best results for Frangi on the images of DRIVE, the parameters are set as follows: Scales: 1-5, scale ratio:1, $\beta_1 = 0.25$ and $\beta_2 = 5$. Frangi filter is a vessel enhancement method. We use the Otsu threshold [25] to convert the gray level to a binary image for Frangi. Except for the above papers, The results of the other methods are taken from respective original papers. It is observed from Table 7 that our approach has the highest performance of segmentation on the DRIVE images. Only the results obtained by Fraz et al. [27] and Dash et al. [5] are close to the proposed algorithm, but the results of the pathological images in the Fraz method are much lower than those of our method. The average accuracy of Fraz for three images (3, 8, 14) of DRIVE is the same as our approach but its average sensitivity is 0.6759 while the average sensitivity of our approach is 0.7406 and it demonstrates that the proposed algorithm is more efficient than Fraz for vessel segmentation in pathological images. Similarly, the average accuracy of [5] for three pathological images is lower than the average accuracy of the proposed algorithm. In a similar way, we have a better performance measure of pathological retinal images than [38]. The average sensitivity of [38] in the pathological images is 0.7181. Although the accuracy of Heneghan is the highest value, Heneghan has the worst values of sensitivity in Table 7. The value of accuracy in our approach based on STARE images is less than other related work, but the proposed algorithm has a higher sensitivity than other algorithms. The authors in [12] obtained the highest sensitivity, in all datasets, while the average of specificity in [12] is the lowest. It shows that this work has low power in pathology detection and noise elimination. The average accuracy of [12] of DRIVE and HRF is lower than our method. In contrast, our average accuracy of CHASEDB1 is lower than [12]. We do not know how the average of AUC is calculated in [12]. AUC is a mean between sensitivity and specificity but in [12] it

is calculated differently. It should be mentioned that the proposed algorithm is less dependent on the training set and although we did not set the parameters for STARE, HRF, and CHASEDB1 datasets, the performance of the proposed algorithms is comparable to the state-of-the-art approaches.

3.3. Comparison in the absence of main vessels

In retinal blood vessel extraction, a major limitation is that thin blood vessels cannot be detected very well, due to lower contrast. On the other hand, most of blood vessels' pixels are thick vessels. Therefore in these images, the accuracy measure depends on thick vessels and it is clear that the percentage of accuracy typically will be high. Similarly, sensitivity is not useful to indicate performance alone. Therefore, we decided to ignore larger vessels by eliminating thick vessels from images of the Drive dataset. In the next step, to exhibit the performance of the detection of thin vessels, we need a new benchmark of the DRIVE database in the absence of thick vessels. To remove thick vessels, the Canny detector is used. Figure 3 illustrates a randomly chosen benchmark of DRIVE and the corresponding new benchmark image. Afterward, we calculated the measures in Table 8 for all the 20 images of the test set of the DRIVE dataset with a new benchmark.

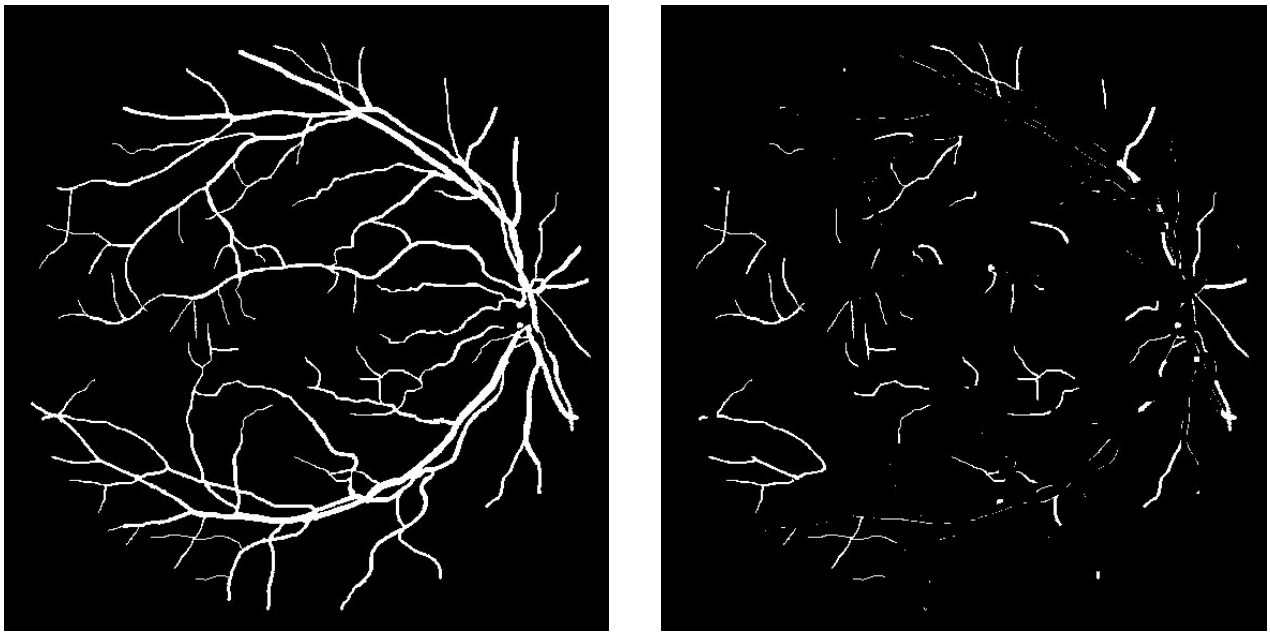

(a) (b)

Figure 3. (a) Expert's annotation, (b) the corresponding new benchmark that made by us.

The average TPR is achieved 0.4544 which means our algorithm can detect 45.44 percent of the thin vessel pixels. The average accuracy, FPR, and informedness are achieved as 0.9616, 0.0164, and 0.4387, respectively. We calculated these five metrics for papers [8, 16, 19, 20, 24], and present them in Table 8. We use Otsu's method for thresholding in all five papers to make a fair comparison. In this section, we use a new measure called J index or informedness. It is obtained as J = sensitivity + specificity – 1. F-score only considers two positive classes (precision and sensitivity) but the J index considers information from both positive and negative classes (sensitivity and specificity). The ability of the algorithms with informedness shows better than TPR alone. It is observed in Table 8 that the J index of the proposed algorithm is higher than the other methods

Table 7. Performance of vessel segmentation methods on the DRIVE, STARE, HRF, and CHASEDB1 databases.

DRIVE							
	Method	Accuracy	TPR	FPR	Sensitivity	Specificity	AUC
Chaudhuri [7]	Match filter	0.8709	0.6326	0.0936	——	——	——
Frangi [24]	Multiscale	0.9244	0.6804	0.0398	0.6808	0.9602	0.8205
Henghen [20]	Morphology	0.9531	0.5456	0.0075	0.5456	0.9925	0.7691
Fraz [27]	Morphology	0.9422	——	——	0.7302	0.9742	0.8522
Nguyen [4]	Multiscale	0.9404	——	——	——	——	——
Zhang [10]	Match filter	0.9382	0.7120	0.0276	——	——	——
Zolfagharnasab [8]	Match filter	0.9269	0.6239	0.0286	——	——	——
Khan [28]	Morphology	0.96075	——	——	0.7462	0.9801	0.8631
Singh [29]	Match filter	0.9522	0.7594	0.0292	——	——	——
Roy [30]	Match filter	0.9295	——	——	0.4392	0.9622	0.7007
Dash [5]	Multiscale	0.9496	——	——	0.7314	0.9891	0.8602
Shukla [31]	Match filter	0.9476	——	——	0.7015	0.9836	0.8426
Soares [32]	Multiscale	0.9461	——	——	0.7332	0.9782	——
Melinscak [11]	CNN	0.9466	0.7276	0.0215	——	——	——
Shin [12]	CNN	0.9271	——	——	0.9382	0.9255	0.9802
Proposed algorithm	Active contour	0.9430	0.7333	0.0259	0.7336	0.9741	0.8539
STARE							
Fraz [27]	morphology	0.9423	——	——	0.7318	0.9660	0.8489
Nguyen [4]	Multiscale	0.9324	——	——	——	——	——
Zhang [10]	Match filter	0.9484	0.7177	0.247	——	——	——
Khan [28]	Morphology	0.94585	——	——	0.75805	0.9627	0.8604
Singh [29]	Match filter	0.9270	0.7939	0.0624	——	——	——
Roy [30]	Match filter	0.9488	——	——	0.4317	0.9718	0.7018
Gao [6]	Multiscale	0.9401	——	——	0.7581	0.9550	08566
Shukla [31]	Match filter	0.9573	——	——	0.7023	0.9863	0.8443
Soares [32]	Multiscale	0.9479	——	——	0.7202	0.9747	——
Shin [12]	CNN	0.9378	——	——	0.9598	0.9352	0.9877
Proposed algorithm	Active contour	0.9372	0.7829	0.0447	0.7831	0.9553	0.8692
HRF							
	Method	Accuracy	TPR	FPR	Sensitivity	Specificity	AUC
Shin [12]	CNN	0.9349	——	——	0.9546	0.9329	0.9838
Proposed algorithm	Active Contour	0.9432	——	——	0.7882	0.9596	0.8738
CHASEDB1							
	Method	Accuracy	TPR	FPR	Sensitivity	Specificity	AUC
Shin [12]	CNN	0.9373	——	——	0.9463	0.9329	0.983
Proposed algorithm	Active Contour	0.9239	——	——	0.8	0.9365	0.8683

with a lot of difference. The active contour based on intensity inhomogeneities [16] has the lowest value of the informedness index by 0.0191.

Table 8. Performance of vessel segmentation methods on the DRIVE database in the absence of wide vessels.

	ACC	TPR	FPR	Informedness
Frangi [24]	0.9514	0.3271	0.0215	0.3062
Henghen [20]	0.9712	0.0877	0.0027	0.085
Intensity inhomogeneities [16]	0.9105	0.0647	0.0457	0.0191
Zolfagharnasab [8]	0.9005	0.3556	0.0757	0.2805
Chan-Vese [19]	0.9610	0.3319	0.0070	0.3253
Proposed algorithm	0.9616	0.4544	0.0164	0.4387

4. Conclusion

In this paper, a blood vessel segmentation based on a modified active contour of the retinal images is presented. In this work, firstly, a preprocessing phase to improve the contrast between vessels and background was performed. Then vessel enhancement filter with morphologies operators and second derivation Gaussian is used to increase the contrast and decrease intensity inhomogeneities and noises. In the next step, we increased the performance of the active contour with changing energy formula. We proposed an improved energy function using discrete wavelet transform to solve the problem of the false detection rate. In addition, we introduced the optimization process phase that improved the performance of the proposed algorithm. The result of the proposed algorithm is better than other works. To more demonstrate the performance of our approach, we compute evaluation metrics in the absence of main vessels. The results demonstrated our approach is comparable to the state-of-the-art approaches.

References

[1] Fraz MM, Remagnino P, Hoppe A, Uyyanonvara B, Rudnicka AR et al. Blood vessel segmentation methodologies in retinal images – A survey. Computer Methods and Programs in Biomedicine 2012; 108 (1): 407-433. doi: 10.1016/j.cmpb.2012.03.009

[2] Kirbas C, Quek F. A review of vessel extraction techniques and algorithms. ACM Computing Surveys (CSUR) 2004; 36 (2): 81-121. doi: 10.1145/1031120.1031121

[3] Wang Y, Ji G, Lin P, Trucco E. Retinal vessel segmentation using multiwavelet kernels and multiscale hierarchical decomposition. Pattern Recognition 2013; 46 (8): 2117-2133. doi: 10.1016/j.patcog.2012.12.014

[4] Nguyen UT, Bhuiyan A, Park LA, Ramamohanarao K. An effective retinal blood vessel segmentation method using multi-scale line detection. Pattern recognition 2013; 46 (3): 703-715. doi: 10.1016/j.patcog.2012.08.009

[5] Dash S, Senapati MR. Enhancing detection of retinal blood vessels by combined approach of DWT, Tyler Coye and Gamma correction. Biomedical Signal Processing and Control 2020; 57: 101740. doi: 10.1016/j.bspc.2019.101740

[6] Gao J, Chen G, Lin W. An effective retinal blood vessel segmentation by using automatic random walks based on centerline extraction. BioMed Research International 2020; 2020: 7352129. doi: 10.1155/2020/7352129

[7] Chaudhuri S, Chatterjee S, Katz N, Nelson M, Goldbaum M. Detection of blood vessels in retinal images using two-dimensional matched filters. IEEE Transactions on medical imaging 1989; 8 (3): 263-269. doi: 10.1109/42.34715

[8] Zolfagharnasab H, Naghsh-Nilchi AR. Cauchy based matched filter for retinal vessels detection. Journal of Medical Signals and Sensors 2014; 4(1): 1.

[9] Singh NP, Srivastava R. Retinal blood vessels segmentation by using Gumbel probability distribution function based matched filter. Computer Methods and Programs in Biomedicine 2016; 129: 40-50. doi: 10.1016/j.cmpb.2016.03.001

[10] Zhang B, Zhang L, Zhang L, Karray F. Retinal vessel extraction by matched filter with first-order derivative of Gaussian. Computers in Biology and Medicine 2010; 40 (4): 438-445. doi: 10.1016/j.compbiomed.2010.02.008

[11] Melinscak M, Prentasic P, Loncaric S. Retinal Vessel Segmentation using Deep Neural Networks. in VISAPP 2015; doi: 10.5220/0005313005770582

[12] Shin SY, Lee S, Yun ID, Lee KM. Deep vessel segmentation by learning graphical connectivity. Medical Image Analysis 2019; 58: 101556. doi: 10.1016/j.media.2019.101556

[13] Li Q, Feng B, Xie L, Liang P, Zhang H et al. A cross-modality learning approach for vessel segmentation in retinal images. IEEE transactions on medical imaging 2015; 35 (1): 109-118. doi: 10.1109/TMI.2015.2457891

[14] Lázár I, Hajdu A. Segmentation of retinal vessels by means of directional response vector similarity and region growing. Computers in biology and medicine 2015; 66 (11): 209-221. doi: 10.1016/j.compbiomed.2015.09.008

[15] Zhao YQ, Wang XH, Wang XF, Shih FY. Retinal vessels segmentation based on level set and region growing. Pattern Recognition 2014; 47 (7): 2437-2446. doi: 10.1016/j.patcog.2014.01.006

[16] Li C, Huang R, Ding Z, Gatenby JC, Metaxas DN et al. A level set method for image segmentation in the presence of intensity inhomogeneities with application to MRI. IEEE Transactions on Image Processing 2011; 20 (7): 2007-2016. doi: 10.1109/TIP.2011.2146190

[17] Al-Diri B, Hunter A, Steel D. An Active Contour Model for Segmenting and Measuring Retinal Vessels. IEEE Transactions on Medical Imaging 2009; 28 (9): 1488-1497. doi: 10.1109/TMI.2009.2017941

[18] Zhao Y, Rada L, Chen K, Harding SP, Zheng Y. Automated vessel segmentation using infinite perimeter active contour model with hybrid region information with application to retinal images. IEEE Transactions on Medical Imaging 2015; 34 (9): 1797-1807. doi: 10.1109/TMI.2015.2409024

[19] Chan TF, Vese LA. Active contours without edges. IEEE Transactions on image processing 2001; 10 (2): 266-277. doi: 10.1109/83.902291

[20] Heneghan C, Flynn J, O'Keefe M, Cahill M. Characterization of changes in blood vessel width and tortuosity in retinopathy of prematurity using image analysis. Medical image analysis 2002; 6 (4): 407-429. doi: 10.1016/S1361-8415(02)00058-0

[21] Mumford D, Shah J. Optimal approximations by piecewise smooth functions and associated variational problems. Communications on pure and applied mathematics 1989; 42 (5): 577-685. doi:10.1002/cpa.3160420503

[22] Crandall R. Image segmentation using the Chan–Vese algorithm. in Project report from ECE 2009.

[23] Mallat S. A theory for multiresolution signal decomposition: The wavelet representation. IEEE Transactions on Pattern Analysis and Machine Intelligence 1989; 11 (7): 674-693. doi: 10.1515/9781400827268.494

[24] Frangi AF, Niessen WJ, Vincken KL, Viergever MA. Multiscale vessel enhancement filtering, in Medical Image Computing and Computer-Assisted Intervention — MICCAI'98: First International Conference Cambridge, MA, USA, October 11–13, 1998 Proceedings. Wells W.M, Colchester A, Delp S. Editors. Springer Berlin Heidelberg: Berlin, Heidelberg, 1998, pp. 130-137. doi: 10.1007/BFb0056195

[25] Otsu N. A threshold selection method from gray-level histograms. Automatica 1975; 11 (285-296): 23-27.

[26] Odstrcilik J, Kolar R, Budai A, Hornegger J, Jan J et al. Retinal vessel segmentation by improved matched filtering: evaluation on a new high-resolution fundus image database. IET Image Processing 2013; 7 (4): 373-383. doi:10.1049/iet-ipr.2012.0455

[27] Fraz MM, Basit A, Barman S. Application of morphological bit planes in retinal blood vessel extraction. Journal of digital imaging 2013; 26 (2): 274-286. doi: 10.1016/j.cmpb.2012.03.009

[28] BahadarKhan K, A Khaliq A, Shahid M. A Morphological Hessian Based Approach for Retinal Blood Vessels Segmentation and Denoising Using Region Based Otsu Thresholding. PLOS ONE 2016; 11 (7): e0158996. doi: 10.1371/journal.pone.0158996

[29] Singh NP, Srivastava R. Retinal blood vessels segmentation by using Gumbel probability distribution function based matched filter. Computer Methods and Programs in Biomedicine 2016; 129 (6): 40-50. doi: 10.1016/j.cmpb.2016.03.001

[30] Roy S, Mitra A, Roy S, Setua SK. Blood vessel segmentation of retinal image using Clifford matched filter and Clifford convolution. Multimedia Tools and Applications 2019; 78 (24): 34839-34865. doi: 10.1007/s11042-019-08111-0

[31] Shukla AK, Pandey RK, Pachori RB. A fractional filter based efficient algorithm for retinal blood vessel segmentation. Biomedical Signal Processing and Control 2020; 59: 101883. doi: 10.1016/j.bspc.2020.101883

[32] Soares JV, Leandro JJ, Cesar RM, Jelinek HF, Cree MJ. Retinal vessel segmentation using the 2-D Gabor wavelet and supervised classification. IEEE Transactions on medical Imaging 2006; 25 (9): 1214-1222. doi: 10.1109/TMI.2006.879967